Magleby G375R 12-21-2021HArchiv.PDF

An ensemble of toxic channel types underlies the severity of the *de novo* variant G375R of the human BK channel

Yanyan Geng[a], Ping Li[b,1], Alice Butler[2], Bill Wang[b], Lawrence Salkoff[b,c], and Karl L. Magleby[a,2]

[a]Department of Physiology and Biophysics, University of Miami Miller School of Medicine Miami FL 33136, USA; [b]Department of Neuroscience and [c]Department of Genetics, Washington University St. Louis, MO 63110, USA.

[1]Present address: Department of OBGYN, Washington University St. Louis, MO 63110, USA.

[2]Corresponding Author: Karl L. Magleby, Department of Physiology and Biophysics, University of Miami Miller School of Medicine, R-430, Miami FL 33136

Email: kmagleby@miami.edu

Author contributions: Y.G., P.L., L.S., and K.L.M. designed research; Y.G., P.L., A.B., B.W., L.S., and K.L.M performed research; Y.G, L.S. and K.L.M. wrote the paper.

Key words: Slo1 channel | Ca^{2+}-activated potassium channel | KCa1.1 | *KCNMA1* | channelopathy | neural development disorder | developmental delay | multiple malformation syndrome | heterozygotic

Abstract

De novo mutations play a prominent role in neurodevelopmental diseases including autism, schizophrenia, and intellectual disability. Many *de novo* mutations are dominant and so severe that the afflicted individuals do not reproduce, so the mutations are not passed into the general population. For multimeric proteins, such severity may result from a dominant-negative effect where mutant subunits assemble with WT to produce channels with adverse properties. Here we study the *de novo* variant G375R heterozygous with the WT allele for the large conductance voltage- and Ca^{2+}-activated potassium (BK channel, Slo1. This variant has been reported to produce devastating neurodevelopmental disorders in three unrelated children. If mutant and WT subunits assemble randomly to form tetrameric BK channels, then ~6% of the assembled channels would be wild type (WT, ~88% would be heteromeric incorporating from 1-3 mutant subunits per channel, and ~6% would be homomeric mutant channels consisting of four mutant subunits. To test this hypothesis, we analyzed the biophysical properties of the single BK channels in the ensemble of channels expressed following a 1:1 injection of mutant and WT cRNA into oocytes. We found ~3% were WT channels, ~85% were heteromeric channels, and ~12% were homomeric mutant channels. All of the heteromeric channels as well as the homomeric mutant channels displayed toxic properties, indicating a dominant negative effect of the mutant subunits. The toxic channels were open at inappropriate negative voltages, even in the absence of Ca^{2+}, which would lead to altered cellular function and decreased neuronal excitability.

Significance

We examined the molecular basis for a severe channelopathy associated with developmental and neurological disorders for a *de novo* variant of the Ca^{2+}-activated potassium (BK) channel, Slo1. To identify the types of BK channels underlying the pathogenicity of the variant, we recorded from BK channels expressed for the G375R mutation heterozygous with the WT allele. We found five different functional types of BK channels, four of which displayed a gain of function toxicity by shifting channel opening to more negative voltages in proportion to the number of mutant subunits per channel and WT. The aberrant channels would disrupt cellular function and the normal electrical activity of neurons, providing a molecular basis for the severity of the phenotype.

Introduction

The BK channel (Slo1, KCa1.1) is a large conductance K^+ selective channel that is synergistically activated by Ca^{2+} and voltage (1-16). BK channels are homotetrameric proteins comprised of four large alpha subunits >1200 amino acids each encoded by the *KCNMA1* gene (*SI Appendix,* Fig. S1). BK channels are widely expressed in many cell types where they modulate smooth muscle contraction (17), transmitter release (18), circadian rhythms (19), repetitive firing (20), and cellular excitability (21). Mutations in *KCNMA1* produce a wide range of disease, including epilepsy, dyskinesis, autism, multiple congenital abnormalities, developmental delay, intellectual disability, axial hypotonia, ataxia, cerebral and cerebellar atrophy, bone thickening, and tortuosity of arteries (22-26). Studies of the functional properties of the BK channels underlying these phenotypes have typically focused on homotetrameric mutant channels comprised of 4 mutant subunits. Yet, for a mutation heterozygous with the wild-type (WT) allele, mutant and WT subunits may have the potential to assemble in different stoichiometries to produce various types of channels with different properties (25). Support for this possibility comes from experimental observations that suggest that BK channels in chromaffin cells can assemble from two distinct BK subunits that confer different inactivation properties (27), and that BK G354S and WT subunits appear to co-assemble to form channels with activation time constants that fall between those of either channel type alone (28).

Here we show that this is the case for a *de novo* missense mutation in the alpha subunit of BK channels (c.1123G>A; p.G375R) that produced severe neurological disorders in three unrelated children. Individuals that carry this mutation have a syndromic neurodevelopmental disorder associated with severe developmental delay and polymalformation syndrome (24). The G375R mutation, located on the back side of the S6 pore-lining helix of the alpha subunit, replaces the H- side chain of glycine with a large arginine side chain that might be expected to distort the subunit structure as well as add a positive charge (*SI Appendix,* Fig. S1).

The *de novo* G375R mutation was heterozygous with the WT allele in all three afflicted children (24) so that both mutant and WT subunits could theoretically assemble to produce five different channel types based on subunit composition, as detailed in Fig. 1. To assess the pathogenic effect of the mutation on channel properties, we injected a 1:1 mixture of cRNA coding for G375R mutant and WT subunits into oocytes to mimic a *de novo* mutation. Whole cell and macro patch recordings from the ensemble of channels expressed following the 1:1 injection indicated that the G375R variant of BK channels acts as a gain-of-function mutation that shifts channel activation to more negative voltages. A detailed single-channel analysis showed that most (~85%) of the ensemble channels expressed following 1:1 injection were heteromeric, as predicted in Fig. 1 for the random assembly of mutant and WT subunits. The heteromeric channels displayed a wide range of negative shifts in activation properties, indicating that the molecular action of the G375R variant subunit is predominantly through a pronounced dominant negative effect, whereby the assembly of mutant subunits with WT

subunits confers detrimental functional properties. The pathogenic negative shift in activation of BK channels with one or more G375R subunits would be devastating to the normal functions of cells, suggesting a basis for the severity of the phenotype.

Results

G375R subunits left shift BK channel activation

To examine what effect a heterozygous (mutant/WT) *de novo* G375R mutation of the pore forming alpha subunit of BK channels would have on channel function, we first compared macroscopic currents flowing through WT BK channels expressed following injection of WT cRNA into oocytes, to those expressed following injection of a 1:1 mixture of mutant and WT cRNA. Injection of a blank without cRNA served as a control. Voltages were stepped from a holding potential of -80 mV to more negative and more positive voltages to reveal the voltage dependent activation of the expressed BK channels (Fig. 2A; *SI Appendix,* Fig. S2). Voltage steps to +50 mV were required to significantly increase membrane conductance from the opening of WT BK channels following injection of WT cRNA. In contrast, some BK channels were already open at -140 mV following a 1:1 injection of mutant and WT cRNA, and depolarization further increased the response. The aberrant BK channels could be either homomeric mutant channels, heteromeric channels, or both.

The left shift in activation for channels expressed from the 1:1 injection was so pronounced that large numbers of BK channels would be open at voltages near the resting membrane potential of -60 mV. Flux of K^+ through the opened BK channels would act to clamp the membrane potential at the equilibrium potential for K^+, opposing depolarization of the cell, which would decrease excitability and interfere with normal neuronal function. Thus, the G375R variant is a toxic gain of function (GOF) mutation. Evidence of its toxic effect is the broad spectrum of developmental and neurological disorders associated with this *de novo* mutation (24); it is a gain-of-function mutation because less depolarization is required to activate the channels.

To quantify the pathogenic negative shift in the ensemble of BK channels following injection of a 1:1 mixture of G375R and WT cRNA, when compared to WT channels following injection of only WT cRNA, we recorded currents from macro patches of membrane which were excised from oocytes after channel expression. This allowed the composition of the solution at the inner membrane surface to be controlled, which was not the case for the whole cell recordings. For a solution at the intracellular membrane surface containing <0.01 μM Ca^{2+} (~0 Ca^{2+}), WT BK channels did not open appreciably until the membrane potential exceeded 100 mV (black circles), whereas the ensemble of BK channels from the 1:1 injection of G375R and WT cRNA started to open at very negative voltages of -80 mV (Fig. 3B). The mean voltage for half activation (V_h) was 182 ± 5.4 mV (n = 6) for WT BK channels and was 61.5 ± 16 mV (n = 12) for ensemble BK channels from the 1:1 injection, giving a mean left shift in channel activation

of -120 mV for the ensemble channels when compared to WT ($p < 0.0001$). This pathogenic left shift in channel activation was even greater in the presence of 300 µM Ca^{2+} (*SI Appendix,* Fig. S3). The 1:1 injection also decreased the voltage sensitivity, with a slope of 38.5 ± 1.8 (n = 8) mV per e-fold change compared to 23.2 ± 1.36 mV (n = 6) for WT channels ($p < 0.0001$).

The large pathogenic negative shifts in channel activation observed for whole cell recordings following a 1:1 injection of mutant and WT cRNA (Fig. 2, *SI Appendix,* Fig. S2) are thus also observed for macro patch recordings under conditions in which the intracellular solution and Ca^{2+} are controlled (Fig. 3; *SI Appendix*, Fig. S3).

Whole cell and macro patch recordings are useful to show the average response of many hundreds to thousands of BK channels, but they provide limited information about the underlying molecular mechanism for the pathogenic response, because individual channels cannot be studied in such recordings. To investigate mechanism in the following sections, we first consider the potential channel types and frequencies of expression that might be expected for a mutation heterozygous with the WT allele, and then record from individual channels to see if these expectations are met.

Five potential types of BK channels

WT and mutant subunits arising from a heterozygous mutation could potentially assemble into five different types of tetrameric channels based on subunit composition alone, each with potentially different properties (Fig. 1). If it is assumed that there is equal production of mutant and WT subunits, that subunits assemble randomly to form tetrameric channels, and that each assembled channel has the same probability of reaching the surface membrane, then the ensemble of channels expressed following a heterozygous mutation would consist of about 6% WT channels, 25% comprised of 1 mutant and 3 WT subunits, 38% comprised of 2 mutant and 2 WT subunits, 25% comprised of 3 mutant and 1 WT subunit, and 6% homomeric mutant channels. On this basis, 94%, of the expressed channels would be pathogenic, comprised of 88% heteromeric channels with mixed subunits and 6% homomeric mutant channels.

Wide range of V_h for ensemble channels

To explore if multiple channel types contribute to the pathogenic effects of a G375R mutation heterozygous with WT, as predicted by Fig. 1, we used the unique ability of the patch clamp technique (29) to isolate and record from single BK channel molecules in the ensemble of BK channels expressed following a 1:1 injection of mutant and WT cRNA into oocytes. For each individual ensemble channel, single-channel currents were recorded over a range of voltages (Fig. 4 *A*) to obtain plots of open probability (Po) vs. voltage for each channel (Fig. 4 *B*, red curves). Po-V plots of the 33 individual ensemble channels studied had a voltage for half activation (V_h) that ranged from -152 mV to +151 mV, for a span of 303 mV (Fig. 4 *B*, red curves). These 33 ensemble channels could in theory be comprised of five different types of channels based on subunit composition alone (Fig. 1), each with potentially different

properties. The very wide range in V_h among the ensemble channels lends support to the idea that the ensemble channels are comprised of multiple channel types with different voltage activation properties. Effective therapies for the *de novo* G375R mutation heterozygous with WT will need to take this into account.

Identifying the types of ensemble channels

To gain insight into the types of ensemble channels expressed following 1:1 injections of mutant and WT cRNA, the Po-V curves of single ensemble channels were compared to the Po-V curves of single WT channels and single homomeric mutant channels. WT channels were obtained by injecting only WT cRNA, and homomeric mutant channels were obtained by injecting only mutant cRNA. Ensemble channels with V_h values within the range of WT channels would be classified as WT channels with four WT subunits. Ensemble channels with V_h values within the range of homomeric mutant channels would be classified as homomeric mutant channels comprised of four mutant subunits. Ensemble channels with V_h values falling between those of WT and homomeric mutant channels would be classified as heteromeric channels with mixed subunit composition.

WT channels had V_h values that spanned a narrow range from 140 to 176 mV (Fig. 4C, black plots), and homomeric mutant channels had V_h values that ranged from -272 mV to -38 mV (Fig. 4C, blue plots). In contrast to our observation of ready expression of homomeric mutant G375R channels, Liang et al. (24) reported no currents with a different expression system (see Discussion).

The homomeric mutant channels had a surprisingly wide range for channels of presumed identical homomeric mutant subunit composition. The reason for such a wide voltage range in V_h for these homomeric mutant channels is not known, but perhaps channels with four mutant subunits can assume different conformations with markedly different activation properties.

To identify the channel types of the ensemble channels, the Po-V curves of the ensemble channels from Fig. 4B were overlaid on plots of the ranges of the Po-V curves for the WT and homomeric mutant channels in Fig. 4D.

One of the 33 ensemble channels had a Po-V curve that overlapped with the WT channels (Fig. 4D), suggesting that one of the 33 ensemble channels was WT. Four of the ensemble channels had Po-V curves that overlapped with the homomeric mutant channels (Fig. 4D), suggesting that these four ensemble channels were comprised of four mutant subunits. The remaining 28 ensemble channels had Po-V curves that that did not overlap with either WT or homomeric mutant channels (Figs. 4D), suggesting that these 28 ensemble channels were heteromeric channels comprised of mixed mutant and WT subunits (Fig. 1).

Thus, for this sampled group of 33 ensemble channels, ~3% (1/33) were WT, ~85% (28/33) were heteromeric, and ~12% (4/33) were homomeric mutant channels (Fig. 4). Fig. 1 predicts ~6% WT, ~88% heteromeric, and ~6% homomeric mutant channels. Simulations of 1 million different groups of 33 ensemble channels each, assuming equal production of mutant and WT

subunits and random assembly into tetrameric channels, indicated that the experimental observations were not significantly different from the predictions of Fig. 1 (*SI Appendix,* Fig. S4) Thus, for a G375R mutation heterozygous to WT, experimental and theoretical considerations suggest that most (85-88%) of the ensemble channels will be heteromeric, with much smaller fractions of homomeric mutant and WT channels.

Dominant negative effect of G375R

Except for the one ensemble channel assigned as WT, all of the other ensemble channels expressed following 1:1 injections of mutant and WT cRNA gave pronounced left (negative) shifts in voltage activation when compared to WT channels (Fig. 4D). For the 85% of ensemble channels that were heteromeric, the mutant subunits dominated the function of the WT subunits, giving toxic left shifts in activation (Fig. 4D). Thus, the toxic left shifts in heteromeric channels arise from a dominant negative effect of the mutant subunits on WT subunits.

The toxic left shifts were even greater for the ~12% of ensemble channels that were homomeric mutant (Fig. 4D). As homomeric mutant channels lack WT subunits, the homomeric mutant channels would exert their detrimental action, not by the action of mutant subunits on WT subunits as is the case for heteromeric channels, but by producing toxic currents on their own. The combined toxic currents from the ~85% of the ensemble channels that are heteromeric channels and from the ~12% of the ensemble channels that are homomeric mutant channels would then act to counter the actions of the currents from the ~3% of the ensemble channels that are WT BK channels and from the other normal channels.

Macro currents can obscure mechanism

The narrow error bars for the macro currents recorded from whole cells and macro patches (Figs. 2 and 3; Supplemental Figs. S2 and S3) indicate that the mean responses recorded from hundreds to thousands of channels following injection of WT cRNA or a 1:1 injection of mutant and WT cRNA, are repeatable. Narrow error bars do not necessarily indicate that the individual channels underlying a mean response have near identical properties, as this was not the case for the macro currents recorded from the ensemble of channels expressed following 1:1 injections of mutant and WT cRNA, where the underlying ensemble channels would have a very wide range of V_h (Fig. 4B). In spite this of this very wide range, the macro G-V data obtained from ensemble channels in Fig. 3B (red diamonds) are reasonably well approximated by a single Boltzmann function (blue line), but are better described (red line) by assuming five underlying channel types (Fig. 1) as described in the legend to Fig. 3.

Dual action of G375R subunits on V_h and single channel conductance *g*

In addition to the negative shift in activation induced by G375R mutant subunits (Figs. 2-4), the mutant subunits also decreased single-channel conductance (Fig. 5A, B). The mean single-channel conductance of WT channels at 100 mV was 312 ± 4 pS. This decreased to 245 ± 6 pS

for heteromeric channels, and further decreased to 190 ± 14 pS for homomeric mutant channels. These decreases were significant (see Fig. 5 legend). Hence, single-channel conductance decreased as the number of mutant subunits per channel increased.

To examine the relationship between single-channel conductance and V_h, the single-channel conductance was plotted against V_h for that channel in Fig. 5C for the indicated channel types. A linear relationship was observed (Fig. 5C; R = 0.86, P < 0.0001). When taken together, the data in Figs. 5B and 5C are consistent, with the idea that each additional mutant subunit adds both an increment of left shift to V_h and a decrease in single-channel conductance. Thus, at the single-channel level, the *de novo* G375R mutation acts as a GOF mutation to left-shift voltage activation (Figs. 4 and 5) and as a loss-of-function (LOF) mutation to decrease single-channel conductance (Fig. 5). The increased activation and current from the GOF left shifts in V_h would dominate over the decrease in current from the LOF reduction in single-channel conductance, producing pathogenic left shifted currents (Figs. 2 and 3; *SI Appendix,* Figs. S2 and S3).

Multiple types of ensemble channels

If each additional mutant subunit in the tetrameric BK channel adds an increment of left shift in V_h, as suggested in the preceding section, then the V_h values of the ensemble channels might cluster into groups based on the number of mutant subunits per channel. To explore this possibility, a histogram of the number of channels vs. V_h for the ensemble channels in Fig. 4B was plotted in Fig. 6. as red bars. Histograms of WT channels (black) and homomeric mutant channels (blue) from Fig. 4C are also plotted. The subunit compositions of the homomeric mutant and WT channels are known and indicated above the channel types. Four of the ensemble channels had V_h values that overlapped with those of homomeric mutant channels, suggesting they had a subunit composition of four mutant subunits. One ensemble channel overlapped with WT channels, suggesting that it was a WT channel. Ensemble channels with V_h values falling between those of WT and homomeric mutant channels would be heteromeric channels, as they are neither WT nor homomeric mutant channels.

As a working hypothesis, the three different subunit combinations of heteromeric channels (Fig. 1) have been placed between the WT and homomeric mutant channels to obtain a stepwise increase in the number of mutant subunits to systematically bridge the gap between WT and homomeric mutant channels. The decrease in conductance as V_h shifts left (Fig. 5) also supports that the number of mutant subunits increase as V_h shifts negative (Fig. 5). The relative percentages of the different types of ensemble channels in Fig. 6 are consistent to a first approximation with the predictions in Fig. 1 (*SI Appendix,* Fig. S4), lending support to the scheme in Fig. 1 as the molecular basis underlying the pathogenicity of the G375R mutation acting through a dominant negative effect. Whereas the apparent observation of three clusters of V_h values for the heteromeric channels (Fig. 6) is consistent with theoretical predictions for three different subunit combinations of heteromeric channels (Fig. 1), peaks can occur by chance alone in histograms of binned data of limited sample size (30). Consequently, larger sample sizes will

be needed to determine whether V_h values for heteromeric channels can consistently be resolved into peaks, but the observation of such distinct peaks is not required for support of the mechanism in Fig. 1, as experimental variation in values of V_h could obscure such peaks.

Discussion

To characterize the action of the G375R *de novo* mutation in human BK channels, we first examined the mean response of the ensemble of BK channels expressed following a 1:1 injection of G375R mutant and WT cRNA to mimic a mutation heterozygous to the WT allele. Recordings from whole cells and macro patches containing many hundreds to thousands of channels indicated that the voltage required for half activation, V_h, was left shifted to more negative potentials by more than 100 mV compared to WT channels (Figs. 2 and 3; *SI Appendix,* Figs. S2 and S3), indicating a toxic GOF mutation. GOF because much less depolarization is required to activate the BK channels expressed following the 1:1 injection when compared to WT channels. Toxic at the molecular level because the mutant channels would be open at negative potentials where they would inhibit depolarization, and toxic at the organism level because of the devastating phenotypes of malformation syndrome and neurological and developmental disorders (24).

To explore the underlying molecular basis for the negative shift in channel activation, we recorded from single BK channel molecules from the ensemble of BK channels expressed following 1:1 injection of mutant and WT cRNA. We found that ~3% of the ensemble channels were WT, ~85% were heteromeric channels of mixed subunits, and ~12% were homomeric mutant channels. All of the heteromeric and homomeric ensemble channels in our experiments displayed pathogenic negative shifts in activation (Figs. 4-6), indicating that one or more mutant subunits per channel are sufficient to override the normal properties of any WT subunits. Thus, the *de novo* heterozygous G375R mutation with respect to WT would induce its pathogenicity mainly through a dominant negative effect (31).

Dominant negative mutations in BK and other ion channels have been described previously (28, 32-36), but this is the first time to our knowledge that the underling molecular mechanism has been revealed in such detail at the single channel level. For the G375R mutation heterozygous with WT, 85% of the expressed channels were heteromeric, and all these heteromeric channels displayed toxic properties (Figs. 4-6). Hence, heteromeric channels were the dominant class of pathogenic channel, with the pathogenicity increasing with the number of mutant subunits per channel (Figs. 4-6). We also show that the much smaller fraction of homomeric mutant channels (~12%) also contribute to the pathology, with a greater negative shift per channel than the heteromeric channels. The extent to which our dominant negative GOF observations for the *de novo* G375R mutation apply to other heterozygous gain of function mutations will need to be investigated for each mutation. Clearly, LOF variants arising from lack of trafficking would employ different mechanisms (37).

In addition to the GOF left shift in V_h, we also observed a LOF action through a decrease in single channel conductance. The decreased conductance may arise from the large volume and positive charge of the large mutant arginine side chains added to S6, which lines the inner conductance pathway of the BK channel (*SI Appendix,* Fig. S1). The added volume could decrease the volume of the inner vestibule and the added positive charge may act to repel K^+ from the inner cavity. Both actions can reduce single channel conductance in BK channels (38-40).

Our experimental observations for the types and percentages of ensemble channels following a 1:1 injection of mutant and WT cRNA were consistent to a first approximation with the predictions of Fig. 1 (*SI Appendix*, Fig. S4), based on assumptions of equal production of mutant and WT subunits that randomly assemble into channels with equal probability of each assembled channel reaching the surface membrane (Figs. 4, 6; *SI Appendix,* Fig. S4). Experiments with much larger sample sizes than 33 ensemble channels would be needed to further test the assumptions underlying the scheme in Fig. 1.

Our findings that the G375R variant is a pathogenic GOF mutation that mainly acts through a dominant negative effect (Fig. 4) differ from those of Liang et al. (24) who reported that the G375R variant confers LOF. Liang et al. (24) studied BK channels in macro patches excised from HEK293T cells. They found that voltage steps induced currents after transfection with the *KCNMA1* plasmid for WT channels, but not after transfection with the G375R variant plasmid. They did not try a joint transfection with mutant and WT plasmids to mimic a heterozygous mutation. They concluded that the G375R variant abolished the function of BK channels, blocking the potassium current. In contrast, when we injected only G375R cRNA into oocytes we observed a pronounced GOF negative shift in the activation of channels (Fig. 4A and C). The differences in observations with those of Liang et al. (24) are unlikely to arise from the different expression systems, as we have found that both oocytes and HEK293 cells effectively express WT BK channels and also BK channels with various types of mutations (16, 38, 40, 41).

We did observe that injecting sufficient G375R cRNA alone to obtain whole cell and macro patch recordings was detrimental to the oocytes, which had limited lifetimes, perhaps because of the extreme negative shift in activation of the homomeric mutant BK channels (Fig. 4C). Consequently, homomeric mutant channels were not studied in whole cell and macro patch recordings. Injecting the much smaller amounts of G375R used for single-channel recording did not induce this problem, allowing single homomeric mutant channels to be studied (Fig. 4A, C).

Devising therapies for the *de novo* G375R heterozygous mutation will be challenging. Our experimental observations (Figs. 4 and 6) and theoretical calculations (Fig. 1) suggest that most (94 to 97%) of the ensemble channels would be pathogenic, with only 3 to 6% of the ensemble channels WT. The pathogenic channels would consist of multiple channel types, each with vastly different activation properties and smaller differences in conductance (Figs. 4 - 6). Therapies to block or inactivate mutant channels would need to silence the multiple types of pathogenic channels, while leaving any WT channels intact. Even if such selective blockers could be devised, it is unlikely that the remaining 3 to 6% of WT channels would restore normal cellular function. Effective therapies will likely require replacing or silencing the mutant alleles, or

preventing mutant subunits from assembling with themselves or WT subunits if/when such techniques become practical in humans.

Materials and Methods

Constructs. Experiments were performed using the human large conductance calcium-activated potassium (BK) channel (hSlo1) *KCNMA1* transcript: GenBank: U23767.1 (3) for WT, and a G375R mutation was constructed to match the G375R *de novo* variant described by Liang et al. (24). G375R is at the same position as G310 in Tao and MacKinnon (15), which they called the gating hinge residue. They used an alternative transcript missing the first 65 amino acids compared to U23767.1. Overlap extension PCR cloning was used to generate the G375R mutation, which was verified by sequencing. The new construct was linearized downstream of the end of coding and transcribed with T3 using Invitrogen's T3 mMessage mMachine kit to make cRNA. To mimic the effects of a heterozygous mutation, mutant and WT cRNA were mixed in a 1:1 ratio by weight before injection into oocytes.

Recording and binomial predictions. Details for whole-cell, macro patch, and single channel patch clamp recording, as well as using Xenopus oocytes as an expression system, including solutions and the use of the binomial equation to calculate percentages of the different channel types for random assembly of mutant and WT subunits are available in the *SI Appendix.*

Statistics. Error bars in the figures and error estimates in the text are SEM. Significance was determined with the two-tailed *t*-test unless otherwise indicated.

Data Availability. The data for this study are contained in the figures and text of the manuscript and *SI Appendix.*

ACKNOWLEDGMENTS. This work was supported in part by NIH Grant R01-GM114694 to L.S. and K.L.M. We thank Julia Bulova for technical help during the initial phase of this project.

References

1. J. N. Barrett, K. L. Magleby, B. S. Pallotta, Properties of single calcium-activated potassium channels in cultured rat muscle. *J. Physiol* **331**, 211-230 (1982).
2. R. Latorre, C. Vergara, C. Hidalgo, Reconstitution in planar lipid bilayers of a Ca^{2+}-dependent K^+ channel from transverse tubule membranes isolated from rabbit skeletal muscle. *Proc. Natl. Acad. Sci. U. S. A* **79**, 805-809 (1982).
3. D. P. McCobb *et al.*, A human calcium-activated potassium channel gene expressed in vascular smooth muscle. *Am. J. Physiol* **269**, H767-H777 (1995).
4. B. S. Rothberg, K. L. Magleby, Voltage and Ca^{2+} activation of single large-conductance Ca2+-activated K^+ channels described by a two-tiered allosteric gating mechanism. *J. Gen. Physiol* **116**, 75-99 (2000).
5. F. T. Horrigan, R. W. Aldrich, Coupling between voltage sensor activation, Ca^{2+} binding and channel opening in large conductance (BK) potassium channels. *J. Gen. Physiol* **120**, 267-305 (2002).
6. X. M. Xia, X. Zeng, C. J. Lingle, Multiple regulatory sites in large-conductance calcium-activated potassium channels. *Nature* **418**, 880-884 (2002).
7. L. Salkoff, A. Butler, G. Ferreira, C. Santi, A. Wei, High-conductance potassium channels of the SLO family. *Nat. Rev. Neurosci* **7**, 921-931 (2006).
8. F. T. Horrigan, Perspectives on: conformational coupling in ion channels: conformational coupling in BK potassium channels. *J. Gen. Physiol* **140**, 625-634 (2012).
9. Y. Geng, K. L. Magleby, Single-channel kinetics of BK (Slo1) channels. *Front Physiol* **5**, 532 (2014).
10. A. Pantazis, R. Olcese, Biophysics of BK Channel Gating. *Int. Rev. Neurobiol* **128**, 1-49 (2016).
11. R. Latorre *et al.*, Molecular Determinants of BK Channel Functional Diversity and Functioning. *Physiol Rev* **97**, 39-87 (2017).
12. Y. Zhou, H. Yang, J. Cui, C. J. Lingle, Threading the biophysics of mammalian Slo1 channels onto structures of an invertebrate Slo1 channel. *J. Gen. Physiol* **149**, 985-1007 (2017).
13. X. Tao, R. K. Hite, R. MacKinnon, Cryo-EM structure of the open high-conductance Ca^{2+}-activated K^+ channel. *Nature* **541**, 46-51 (2017).
14. R. K. Hite, X. Tao, R. MacKinnon, Structural basis for gating the high-conductance Ca(2+)-activated K^+ channel. *Nature* **541**, 52-57 (2017).
15. X. Tao, R. MacKinnon, Molecular structures of the human Slo1 K^+ channel in complex with beta4. *Elife* **8** (2019).

16. Y. Geng *et al.*, Coupling of Ca^{2+} and voltage activation in BK channels through the alphaB helix/voltage sensor interface. *Proc Natl Acad Sci U S A* **117**, 14512-14521 (2020).
17. R. Brenner *et al.*, Vasoregulation by the beta1 subunit of the calcium-activated potassium channel. *Nature* **407**, 870-876 (2000).
18. R. Robitaille, M. L. Garcia, G. J. Kaczorowski, M. P. Charlton, Functional colocalization of calcium and calcium-gated potassium channels in control of transmitter release. *Neuron* **11**, 645-655 (1993).
19. J. R. M. Harvey, A. E. Plante, A. L. Meredith, Ion Channels Controlling Circadian Rhythms in Suprachiasmatic Nucleus Excitability. *Physiol Rev* **100**, 1415-1454 (2020).
20. N. Gu, K. Vervaeke, J. F. Storm, BK potassium channels facilitate high-frequency firing and cause early spike frequency adaptation in rat CA1 hippocampal pyramidal cells. *J Physiol* **580**, 859-882 (2007).
21. J. R. Montgomery, A. L. Meredith, Genetic activation of BK currents in vivo generates bidirectional effects on neuronal excitability. *Proc Natl Acad Sci U S A* **109**, 18997-19002 (2012).
22. B. Wang, B. S. Rothberg, R. Brenner, Mechanism of increased BK channel activation from a channel mutation that causes epilepsy. *J. Gen. Physiol* **133**, 283-294 (2009).
23. J. Yang *et al.*, An epilepsy/dyskinesia-associated mutation enhances BK channel activation by potentiating Ca^{2+} sensing. *Neuron* **66**, 871-883 (2010).
24. L. Liang *et al.*, De novo loss-of-function KCNMA1 variants are associated with a new multiple malformation syndrome and a broad spectrum of developmental and neurological phenotypes. *Hum Mol Genet* **28**, 2937-2951 (2019).
25. C. S. Bailey, H. J. Moldenhauer, S. M. Park, S. Keros, A. L. Meredith, KCNMA1-linked channelopathy. *J Gen Physiol* **151**, 1173-1189 (2019).
26. J. P. Miller, H. J. Moldenhauer, S. Keros, A. L. Meredith, An emerging spectrum of variants and clinical features in KCNMA1-linked channelopathy. *Channels (Austin)* **15**, 447-464 (2021).
27. J. P. Ding, Z. W. Li, C. J. Lingle, Inactivating BK channels in rat chromaffin cells may arise from heteromultimeric assembly of distinct inactivation-competent and noninactivating subunits. *Biophys J* **74**, 268-289 (1998).
28. X. Du *et al.*, Loss-of-function BK channel mutation causes impaired mitochondria and progressive cerebellar ataxia. *Proc Natl Acad Sci U S A* **117**, 6023-6034 (2020).
29. O. P. Hamill, A. Marty, E. Neher, B. Sakmann, F. J. Sigworth, Improved patch-clamp techniques for high-resolution current recording from cells and cell-free membrane patches. *Pflugers Arch* **391**, 85-100 (1981).
30. D. C. Miller, M. M. Weinstock, K. L. Magleby, Is the quantum of transmitter release composed of subunits? *Nature* **274**, 388-390 (1978).

31. A. O. Wilkie, The molecular basis of genetic dominance. *J Med Genet* **31**, 89-98 (1994).
32. M. Fink *et al.*, Dominant negative chimeras provide evidence for homo and heteromultimeric assembly of inward rectifier K^+ channel proteins via their N-terminal end. *FEBS Lett* **378**, 64-68 (1996).
33. A. B. Ribera, L. M. Pacioretty, R. S. Taylor, Probing molecular identity of native single potassium channels by overexpression of dominant negative subunits. *Neuropharmacology* **35**, 1007-1016 (1996).
34. P. Zerr, J. P. Adelman, J. Maylie, Episodic ataxia mutations in Kv1.1 alter potassium channel function by dominant negative effects or haploinsufficiency. *J. Neurosci* **18**, 2842-2848 (1998).
35. S. D. Silberberg, T. H. Chang, K. J. Swartz, Secondary structure and gating rearrangements of transmembrane segments in rat P2X4 receptor channels. *J Gen Physiol* **125**, 347-359 (2005).
36. E. Hichri, Z. Selimi, J. P. Kucera, Modeling the Interactions Between Sodium Channels Provides Insight Into the Negative Dominance of Certain Channel Mutations. *Front Physiol* **11**, 589386 (2020).
37. M. M. Zarei *et al.*, A novel MaxiK splice variant exhibits dominant-negative properties for surface expression. *J. Biol. Chem* **276**, 16232-16239 (2001).
38. T. I. Brelidze, X. Niu, K. L. Magleby, A ring of eight conserved negatively charged amino acids doubles the conductance of BK channels and prevents inward rectification. *Proc. Natl. Acad. Sci. U. S. A* **100**, 9017-9022 (2003).
39. C. M. Nimigean, J. S. Chappie, C. Miller, Electrostatic tuning of ion conductance in potassium channels. *Biochemistry* **42**, 9263-9268 (2003).
40. Y. Geng, X. Niu, K. L. Magleby, Low resistance, large dimension entrance to the inner cavity of BK channels determined by changing side-chain volume. *J. Gen. Physiol* **137**, 533-548 (2011).
41. X. Niu, K. L. Magleby, Stepwise contribution of each subunit to the cooperative activation of BK channels by Ca^{2+}. *Proc. Natl. Acad. Sci. U. S. A* **99**, 11441-11446 (2002).

Figure legends

Fig. 1. Protein subunits coded by WT and mutant alleles can potentially assemble into five types of tetrameric BK channels based on subunit composition alone. The percentages of expression of the different channel types were calculated with Eqn. 2 in the *SI Appendix* Materials and Methods, which assumes equal numbers of mutant and WT subunits that randomly assemble into tetrameric channels, each with equal probability of reaching the surface membrane. Ensemble channels are defined as the collection of all channels expressed for a mutation heterozygous with the WT allele. With the above assumptions, 6% of the ensemble channels are WT comprised of 4 WT subunits per channel, 88% are heteromeric (mixed subunit) channels, with from 1 to 3 mutant subunits per channel, and 6% are homomeric mutant channels comprised of 4 mutant subunits per channel. Note that 94% of the ensemble channels can be pathogenic, as they contain from 1 to 4 mutant subunits per channel. The listed percentages of 6% and 38% here and throughout the paper have been rounded from the calculated values of 6.25% and 37.5%.

Fig. 2. BK channels expressed in oocytes following injection of a 1:1 mixture of G375R mutant and WT cRNA activate at greatly left shifted negative potentials compared to BK channels expressed following injection of only WT cRNA. (*A*) Whole cell current traces recorded from oocytes with the two-electrode voltage clamp for the indicated injections of cRNA. The whole cell currents were generated by holding the potential at -80 mV and then jumping to voltages ranging from -140 mV to +60 mV in 10 mV increments (1:1) or to +100 mV (WT and Blank). (*B*) Plots of relative conductance versus the voltage of the steps following injection of a 1:1 mixture of mutant and WT cRNA (red diamonds), for injection of WT cRNA alone (black circles), and injection of carrier only (purple triangles). The high conductance at negative potentials would act to drive the membrane potential to about -80 mV, the equilibrium potential of K^+. The currents used to calculate the relative conductance are in *SI Appendix,* Fig. S2. Mean ± SEM, n = 4 in each case.

Fig. 3. Quantifying the mean pathogenic left shift in V_h following injection of a 1:1 mixture of mutant and WT cRNA when compared to injection of only WT cRNA. Data are for ~0 Ca^{2+} at the intracellular side of the membrane (see *SI Appendix,* Materials and Methods). (*A*) Currents recorded from inside-out macro patches of membrane excised from oocytes. For WT channels following injection of only WT cRNA, voltage pulses were from -80 mV to 240 mV with 20 mV steps from a holding potential of -80 mV. For channels expressed following injection of a 1:1 mixture of G375R mutant and WT cRNA, voltage pulses were from -120 to 240 mV with

20 mV steps from a holding potential of -160 mV. The currents are the mean response from the many hundreds to thousands of BK channels in each excised macro patch of membrane. (*B*) G/G_{max} vs. voltage plots following the injection of WT cRNA alone (black circles, n = 6), or 1:1 injection of mutant and WT cRNA (red diamonds, n = 12). The black line through the WT data is a single Boltzmann fit with V_h = 181.3 mV and slope factor *b* = 24.04 mV/e-fold change in Po at low Po. The blue line through the 1:1 data (red diamonds) is a single Boltzmann function with V_h = 59.04 and *b* = 38.06. The red line through the 1:1 data is the sum of 5 Boltzmann functions with: 1) V_h = -75.7 mV, *b* =21.6 mV/e-fold change, fractional area = 0.0547; 2) 1.5, 21.0, 0.236; 3) 54.6, 13.8, 0.316; 4) 96.6, 14.4, 0.244; 5) 155, 14.0, 0.139. These parameters for the 5 summed Boltzmann functions that describe the 1:1 data are generally consistent with the V_h values for the apparent clusters of ensemble channels (Figs. 4D and 6) and theoretical percentages in Fig. 1. Channel activation is left shifted in the whole cell recordings in Fig. 2 compared to the ~0 Ca^{2+} macro patch recordings in this figure, because the resting free Ca^{2+} in the oocytes of a few micromolar left shifts BK channel activation.

Fig. 4. Identifying the types of BK ensemble channels expressed following a 1:1 injection of G375R mutant and WT cRNA. (*A*) Representative single channel recordings from three different single BK channel molecules: WT channel (top row) following injection of WT cRNA; ensemble channel following 1:1 injection of G375R and WT cRNA, (second row); and homomeric G375R mutant channel following injection of G375R cRNA (third row). Recordings are at three different voltages for each channel type. Depolarization activates each channel type with a markedly different V_h of about 140 mV for the WT channel, 6 mV for the ensemble channel, and ~-100 mV for the homomeric G375R mutant channel. Arrows indicate closed channel current levels. (*B*) Plots of Po vs. *V* for 33 single ensemble channels following 1:1 injection of G375R and WT cRNA (red diamonds with Boltzmann fits). (*C*) Plots of Po vs. *V* for 12 single homomeric G375R mutant channels following injection of G375R cRNA (blue squares with Boltzmann fits), and for 9 WT channels following injection of WT cRNA (black circles and Boltzmann fits). (*D*) Identifying the types of ensemble channels. Blue and gray areas indicate the range of observed V_h for G375R mutant channels and WT channels, respectively, from *C*. One of the ensemble channels (rightmost red Po-*V* curve) overlaps with the WT channels (gray shading), indicating that this ensemble channel is likely a WT channel with four WT subunits. Four of the ensemble channels (four leftmost red Po-*V* curves) overlap with the G375R mutant channels (blue shading) indicating that these 4 ensemble channels are likely homomeric G375R channels assembled from 4 mutant subunits. The remaining 28 ensemble channels would be heteromeric channels with mixed subunits, as their V_h values do not overlap with those of either homomeric mutant or WT channels.

Fig. 5. Each additional G375R mutant subunit in a BK channel acts both to left shift V_h to more negative potentials and decrease single channel conductance. (*A*) Currents recorded from single channels at +100 mV after injecting the indicated cRNA. (*B*) Single-channel conductance at +100 mV decreases as the number of mutant subunits increase. Mean single-channel conductance for WT channels was 312 ± 4 pS (n = 7), decreasing to 245 ± 6 pS for heteromeric channels (n = 25, $p < 0.0001$), and further decreasing to 190 ± 14 pS for homomeric G375R channels (n = 8, p = 0.0003). Mean ± SEM. The WT channels included for the mean WT conductance were those channels expressed after injecting only WT cRNA. The homomeric mutant channels included for the mean homomeric mutant conductance were those channels expressed after injecting only G375R mutant cRNA. The heteromeric channels included for the mean heteromeric conductance were identified as in Fig. 4D. WT channels would have 4 WT subunits, heteromeric channels have mixed subunits of three differ combinations: 1 mutant/3 WT, 2 mutant/2 WT, and 3 mutant/1 WT, and G375R channels have 4 mutant subunits. (*C*) Plot of single channel conductance at +100 mV vs. V_h for BK channels expressed following injection of the indicated cRNA. The linear regression line relates single channel conductance (g) to V_h, where: $g = V_h(0) + aV$, where $V_h(0)$ = 231.9 ± 3.9 pA and a = 0.408 ± 0.0375 pS/mV ($p < 0.0001$ for a slope different from 0). R = 0.86.

Fig. 6. The observed numbers of the types of ensemble channels appear consistent, to a first approximation, with the theoretical predictions in Fig. 1. Histograms of V_h values of single channels from Fig. 4. Ensemble channels from 1:1 injection of mutant and WT cRNA are indicated by red bars. WT channels from injection of only WT cRNA are indicated by black bars, and G375R channels from injection of only G375R cRNA are indicated by blue bars. Ensemble channels with V_h values between the blue bars and black bars would be heteromeric ensemble channels of mixed subunits. Red bars interspaced between blue bars would be ensemble channels comprised of four mutant subunits. The red bar in the cluster of black bars would be an ensemble channel comprised of four WT subunits. Hypothesized subunit compositions of the different apparent clusters of channels based on V_h values are indicated. *SI Appendix*, Fig. S4 compares observed and predicted data.

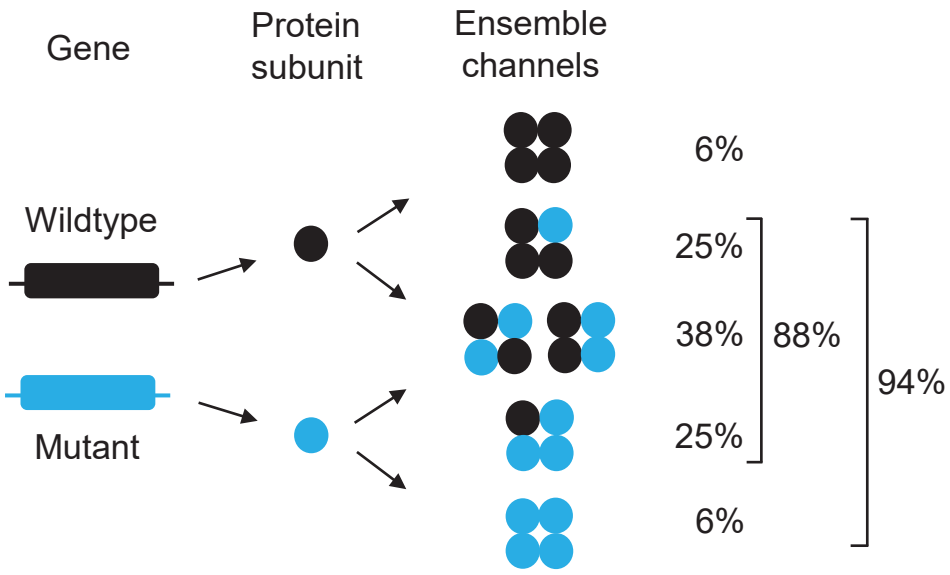

Figure 1

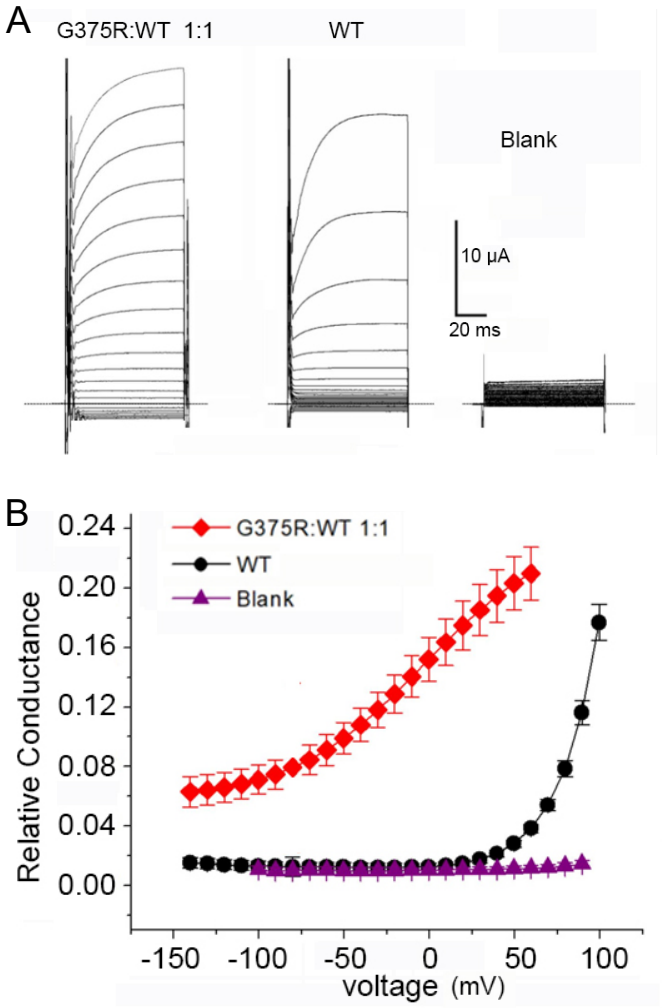

Figure 2

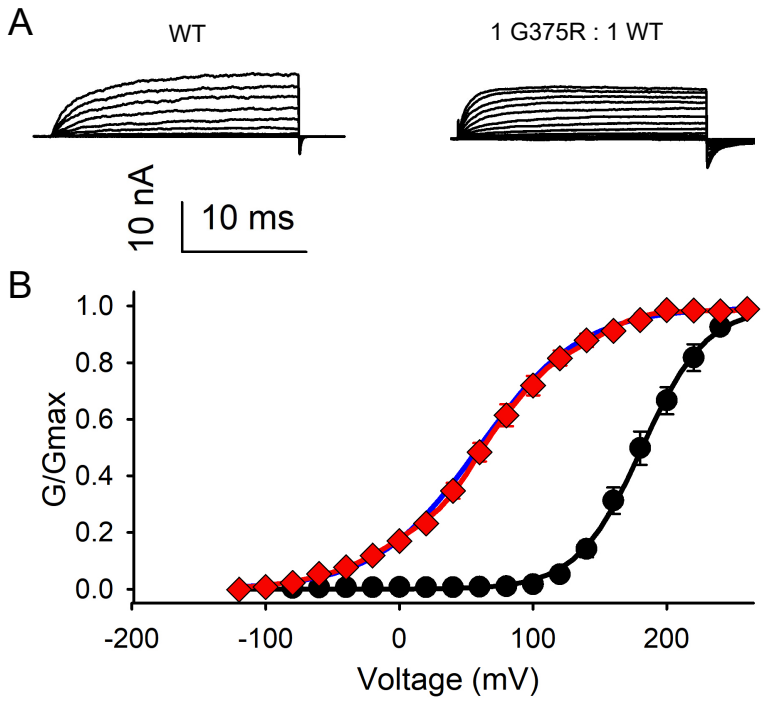

Figure 3

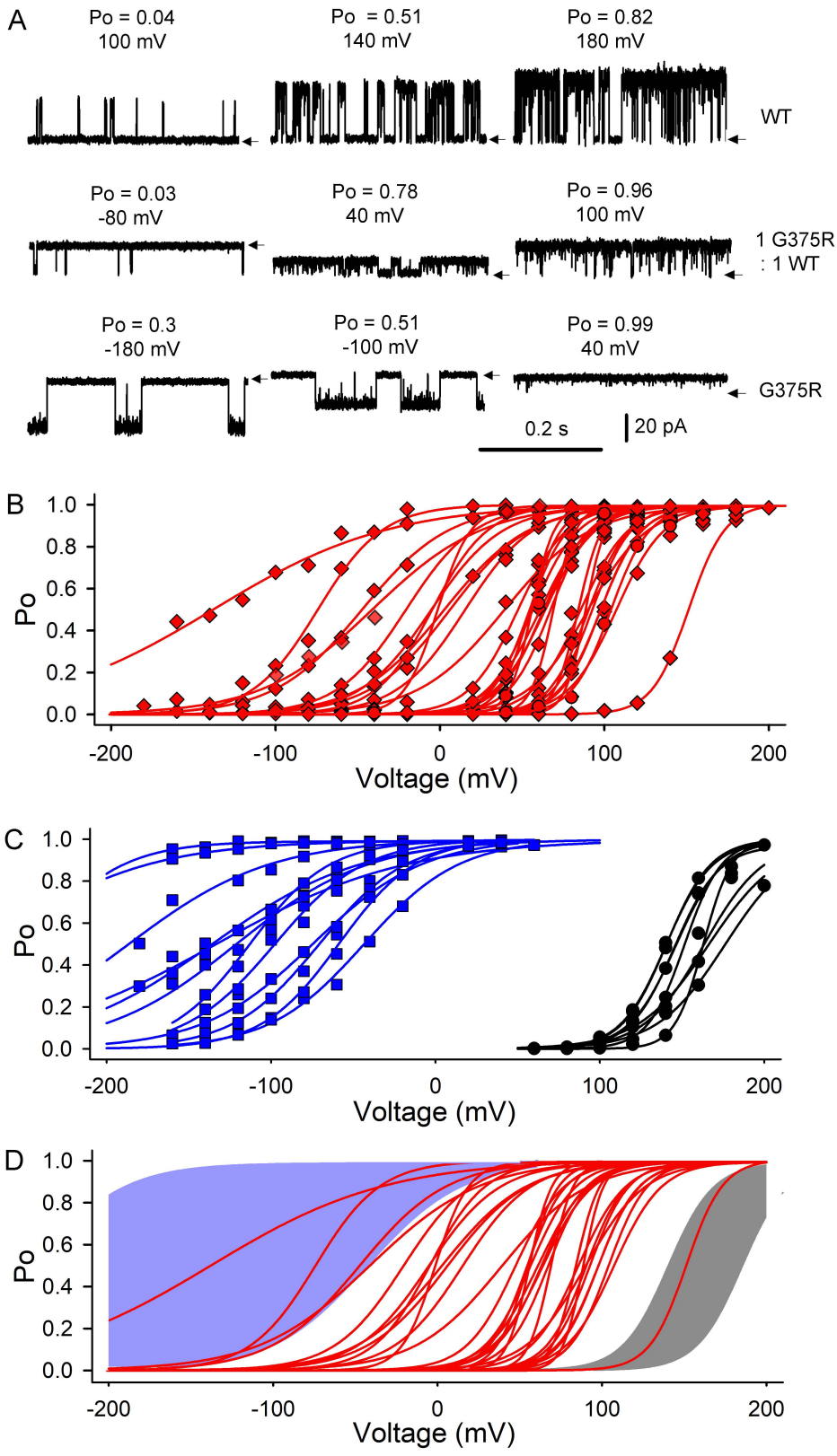

Figure 4

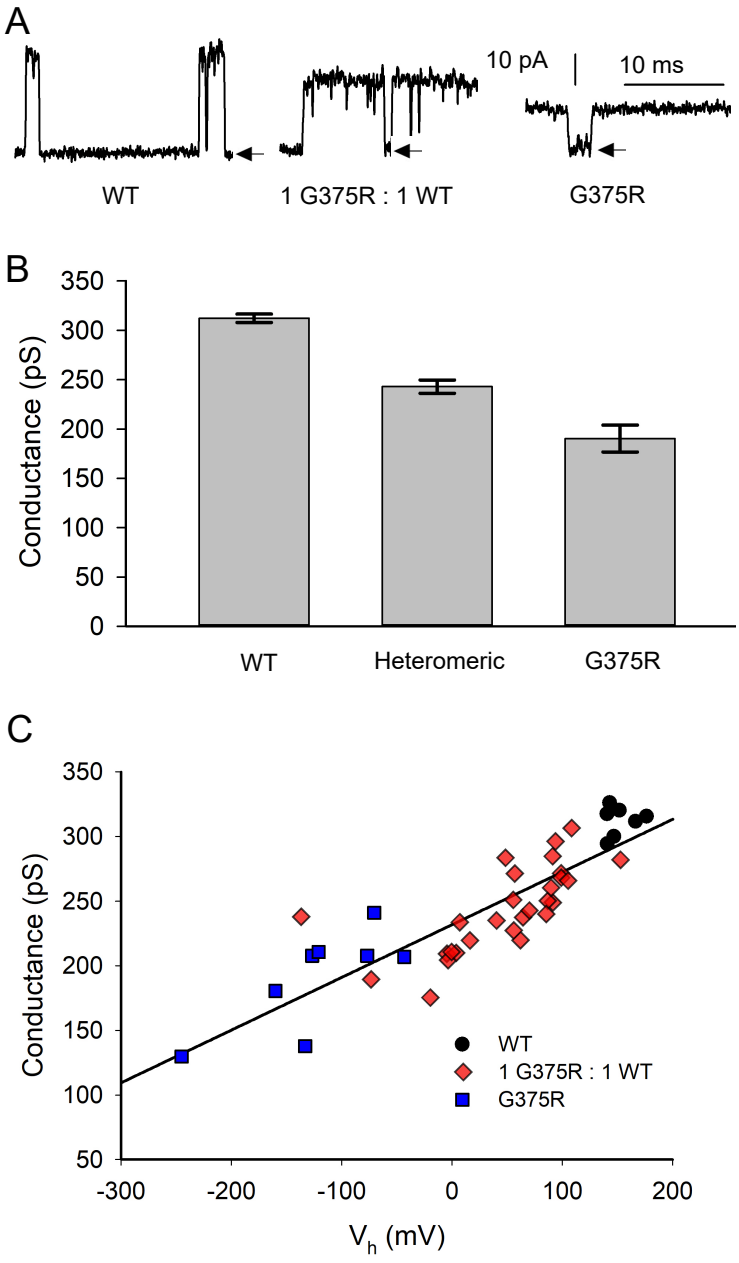

Figure 5

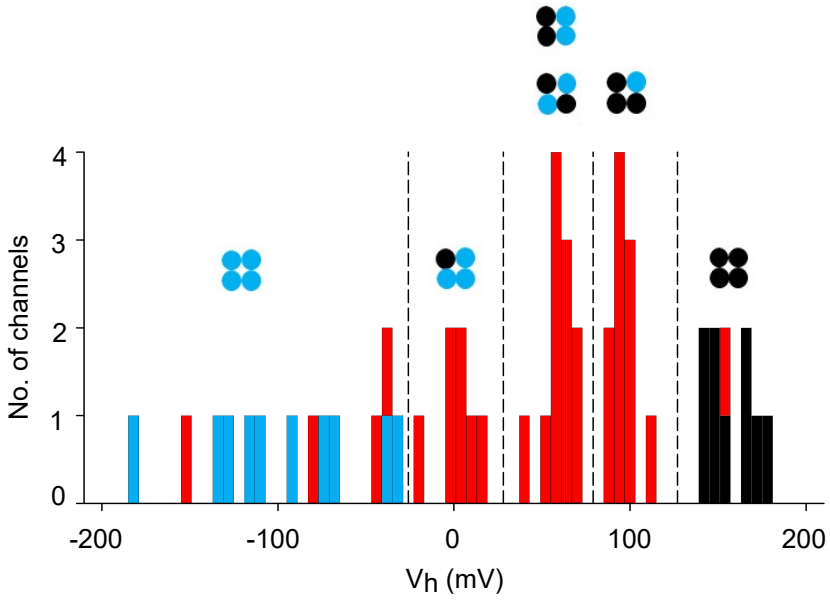

Figure 6